Received: 4 September 2020 | Revised: 16 October 2021 | Accepted: 24 October 2021

DOI: 10.1002/asjc.2744

RESEARCH ARTICLE

WILEY

Neural network-based continuous finite-time tracking control for uncertain robotic systems with actuator saturation

Yi Li[1,2] | Huayang Sai[1,2] | Mingchao Zhu[1] | Zhenbang Xu[1] | Deqiang Mu[3]

[1]Changchun Institute of Optics, Fine Mechanics and Physics, Chinese Academy of Sciences, Changchun, China

[2]University of Chinese Academy of Sciences, Beijing, China

[3]Department of Mechanical Engineering, Changchun University of Technology, Changchun, China

Correspondence
Mingchao Zhu, Changchun Institute of Optics, Fine Mechanics and Physics, Chinese Academy of Sciences, No 3888 Dong Nanhu Road, Changchun 130033, China.
Email: mingchaozhu@gmail.com

Funding information
Jilin Scientific and Technological Development Program, Grant/Award Number: 20200404204YY; National Natural Science Foundation of China, Grant/Award Number: 11672290

Abstract

This paper proposes a neural network-based continuous finite-time tracking controller for the robust high-precision control of robotic systems under model uncertainty, external disturbance, and actuator saturation. First, a fast nonsingular integral terminal sliding mode (FNITSM) surface is adopted to ensure singularity avoidance and fast finite-time convergence. Considering the presence of model uncertainties and external disturbance, the fully adaptive radial basis function neural network (ARBFNN) is used to approximate and compensate for the unknown dynamic model. Then, a novel continuous fast fractional-order power (CFFOP) approach law is explored to increase the convergence rate and eliminate chattering in the FNITSM control. Meanwhile, the approach law relaxes the requirement on the exact information of the upper bound of the disturbances and their time derivatives. Besides, an actuator saturation compensator (ASO) is proposed to compensate for the limited control input. The stability and finite-time convergence of the proposed controller are analyzed using the Lyapunov theory. Finally, comparative simulations of both the numerical and application examples are conducted to verify the effectiveness of the proposed control schemes, indicating that the CFFOP approach law and ASO can be used effectively for robotic systems.

KEYWORDS

actuator saturation, continuous finite-time convergence, neural network, nonsingular integral terminal sliding mode, robotic systems

1 | INTRODUCTION

During recent years, there have been many control schemes for robot high-precision tracking control, especially for space manipulators [1], industrial manipulators [2] and surgical robots [3]. The problems associated with the robust high-precision robotic systems control are mainly model uncertainties, external disturbances, and actuator saturation. To deal with these problems, several control methods have been proposed, such as adaptive control [4], sliding mode control (SMC) [5], disturbance observers (DOBs) [6], and neural network (NN) control [7]. Among these approaches, SMC is a simple and powerful tracking control strategy for its strong robustness and fast transient response.

However, conventional SMC only enables the system states converge to equilibrium. Then, more advanced techniques such as terminal SMC (TSMC) [8] were

developed to achieve finite-time convergence of the tracking error. Besides, fast terminal SMC (FTSMC) is investigated in Ahmed et al. [9] to obtain a fast convergence rate. On the other hand, TSMC and FTSMC suffer from singularity problems due to the existence of negative fractional power in controller design. Considering this issue, a nonsingular TSMC (NTSMC) [10] and a nonsingular FTSMC (NFTSMC) [11] have been proposed to avoid the singularity. Meanwhile, a nonsingular integral TSMC (NITSMC) [12] is proposed to eliminate reaching time to the sliding surface compared to the TSMC. In Li et al. [13], a fast NITSMC (FNITSMC) is designed to improve the convergence rate of the NITSMC. Comparing FNITSMC and NITSMC, FNITSMC achieves fast finite-time convergence. Subsequently, an adaptive FNITSMC (AFNITSMC) [14] and an adaptive second-order NTSMC (SONTSMC) [15] is established to attenuate the effect of chattering and improve stability through adaptive disturbance boundaries. Furthermore, time-synchronized control is developed in Li et al. [16,17] to yield simultaneous-arrival-to-origin convergence. The control scheme aims to promote all system states arriving at the origin at the same time.

Noting the premise of some control schemes can be realized is that the robot actuator can provide any theoretically calculated torque. When the theoretically calculated torque exceeds the maximum torque that the actuator can provide, it would fail to reach the theoretically satisfactory tracking or deteriorate the control performance. The problem has been tried to solve with saturation function or standard arc tangent function. And the output of system is still above the saturation zone, and it may still produce overshoot or instability. Subsequently, an auxiliary system is proposed in Zhou et al. [18] and Chen et al. [19] through disturbance observer and used as the overshoot compensation of the spacecraft actuator. In Jiang et al. [20], a fixed-time controller in the presence of actuator saturation and faults is designed to obtain faster convergence with higher accuracy. Besides, an effective method of introducing an auxiliary system and approximating the unknown model through the RBFNN is proposed by Jia and Shan [1] to achieve the finite-time tracking control of the space manipulator. These methods perform better for actuator saturation in TSMC. The downside is that the discontinuous switching function with a high gain may inevitably cause a chattering phenomenon.

Some researchers propose second-order sliding mode control (SOSMC) [15,21] to eliminate chattering further. The controllers need the acceleration signal, which is not easy to obtain or inaccurate due to the noise. Additionally, the disturbance observer is a promising technique to overcome the lumped uncertainty, improve the robustness, and alleviate the chattering of the controller. In Rosas Almeida et al. [22], a disturbance observer is introduced and used as the compensation of the uncertain pneumatic actuators. In Wu et al. [23], the adaptive algorithm is developed to estimate the upper bound of the uncertainties. However, the methods are more suitable for the lumped uncertainty with a bounded time derivative [6]. In Wu et al. [23], a dynamic feedback-linearization method with an extended high-gain observer is proposed to overcome the robustness issues. When the uncertain terms are completely unknown, some intelligent algorithms, including fuzzy control [24], reinforcement learning control [25], and RBFNNs [26], are adopted to approximate and the dynamic uncertainties. In Tran and Kang [27], an adaptive RBFNN (ARBFNN)-based NTSMC is developed for uncertain robotic systems. Benefits from the adaptive laws, the weights, centers, and widths of the ARBFNN can be adjusted in real-time through tracking error. Moreover, a control strategy for the output synchronization network systems via L2-gain analysis is proposed in Wu and Lu [28] to guarantee the security of network systems. In Ma and Huang [29], an adaptive neural-network controller is proposed to reduce the adverse effect arising from input saturation, and the neural network is implemented to approximate the unmodeled dynamics. Therefore, the adaptive neural-network-based sliding mode control with limited control input is a reasonable solution for robust high-precision control of robotic systems.

Given the remarkable benefits and limitations, an attempt is made in this paper to propose a continuous finite-time tracking controller for robotic systems with finite-time convergence in the presence of external disturbances, dynamic model uncertainties and actuator saturation. This paper proposes a comprehensively scheme to promote the performance of FNITSMC with CFFOP, ARBFNN and ASO. The main contributions of this paper are as follows:

- A novel continuous FNITSMC scheme is proposed based on the FNITSM surface and the CFFOP approach law, which ensures fast finite-time convergence without requirement of exact information about the upper bound on the disturbances and their time derivatives;
- For the FNITSMC, the actuator saturation is compensated with the ASO, which guarantees the tracking performance of the system and reduces the energy consumption.
- The ARBFNN technique is used to online compensate for the lumped uncertainties of robotic systems. Benefits from the CFFOP, ASO, and ARBFNN, the control

scheme promotes the FNITSMC's performance development.

The rest of this paper is organized as follows. Section 2 formulates the problem and gives preliminaries and notations. Sections 3 introduces the design of ARBFNN based FNITSMC scheme. Section 4 presents the proposed CFFOP approach law. The simulation results for a two-link robot are given in Section 5 to verify the effectiveness of the proposed algorithms. Finally, the conclusions are given in Section 6.

2 | PROBLEM FORMULATION

2.1 | Preliminaries and notations

The vector $\mathrm{sig}(x)^{\alpha} \in R^n$ is defined as

$$\mathrm{sig}(x)^{\alpha} = |x|^{\alpha}\mathrm{sign}(x) = [|x_1|^{\alpha}\mathrm{sign}(x_1), \cdots, |x_n|^{\alpha}\mathrm{sign}(x_n)]^T. \tag{1}$$

The time derivative of $\mathrm{sig}(x)^{\alpha}$ is

$$\frac{d}{dt}(\mathrm{sig}(x)^{\alpha}) = \alpha|x|^{\alpha-1}\dot{x}, \alpha \geqslant 1. \tag{2}$$

The saturation function is defined as

$$\mathrm{sat}(x) = \begin{cases} \mathrm{sign}(x)x_{\max}, |x| \geqslant x_{\max}, \\ x, |x| < x_{\max}. \end{cases} \tag{3}$$

Lemma 1. (Zhu et al. [8]). For a system $\dot{x} = f(x,u)$, suppose there is continuous function $V(x)$, scalars $\kappa > 0$, $0 < \lambda < 1$, and $0 < \eta < \infty$ such that

$$\dot{V}(x) \leqslant -\kappa V^{\lambda}(x) + \eta. \tag{4}$$

Then the system is local finite-time stable and the settling time satisfies

$$T(x_0) \leqslant \frac{V(x_0)^{1-\lambda}}{\kappa(1-\lambda)}, \tag{5}$$

where $V(x_0)$ is the initial value of $V(x)$.

2.2 | The dynamic model of robot manipulators

The dynamic model of a robotic system can be written as

$$M(q)\ddot{q} + C(q,\dot{q})\dot{q} + G(q) + f_d\dot{q} + f_s(\dot{q}) + \tau_d = \tau_m, \tag{6}$$

where q, $\dot{q}$, and $\ddot{q} \in R^{n\times 1}$ are joint's angular position, velocity, and acceleration, respectively; $M(q) \in R^{n\times n}$ is the symmetric and positive definite inertia matrix; $C(q,\dot{q}) \in R^{n\times n}$ is the matrix of centrifugal and Coriolis terms; $G(q) \in R^{n\times 1}$ is the gravity vector; $f_d \in R^{n\times n}$ denotes the viscous friction coefficient; $f_s(\dot{q}) \in R^{n\times 1}$ is the vector of Coulomb friction term; $\tau_m \in R^{n\times 1}$ represents the input torque vector; and $\tau_d \in R^{n\times 1}$ denotes an unknown vector of the bounded external disturbance. Practically, the parameters of these dynamic terms are hard to get exactly because of modeling error, payload variations, external disturbances, and other factors. Hence, it is assumed that the dynamic model consists of inherent uncertainties. And Equation 6 can be rewritten as

$$\begin{cases} \widehat{M}(q)\ddot{q} + \widehat{C}(q,\ddot{q})\dot{q} + \widehat{G}(q) + \widehat{f}_d\dot{q} + \widehat{f}_s(\dot{q}) + F(q,\dot{q},\ddot{q}) + \tau_d = \tau_m, \\ F(q,\dot{q},\ddot{q}) \coloneqq \Delta f_d\dot{q} + \Delta f_s(\dot{q}) + \Delta M(q)\ddot{q} + \Delta C(q,\dot{q})\dot{q} + \Delta G(q), \end{cases} \tag{7}$$

where the notations $\widehat{M}(q)$, $\widehat{C}(q,\dot{q})$, $\widehat{G}(q)$, $\widehat{f}_d$, and $\widehat{f}_s(\dot{q})$ are the nominal matrices; $\Delta M(q)$, $\Delta C(q,\dot{q})$, $\Delta G(q)$, Δf_d, and $\Delta f_s(\dot{q})$ denote the unknown parts of $M(q)$, $C(q,\dot{q})$, $G(q)$, f_d, and $f_s(\dot{q})$, respectively.

Then, from Equation 7, the simplified dynamical model can be written as

$$\ddot{q} = \widehat{M}^{-1}(q)\left[\tau_m - \widehat{C}(q,\dot{q})\dot{q} - \widehat{G}(q) - \widehat{f}_d\dot{q} - \widehat{f}_s(\dot{q}) - F(q,\dot{q},\ddot{q}) - \tau_d\right]. \tag{8}$$

The tracking error and auxiliary error are defined as

$$\begin{cases} e_1 = q_r - q, \\ e_2 \coloneqq \dot{e}_1(t) + p_1e_1(t), \\ e_s \coloneqq \dot{q}_r(t) + p_1e_1(t), \end{cases} \tag{9}$$

where $p_1 \in R^{n\times n}$ is a positive-definite diagonal matrix. It is noteworthy that the p_1 can be turned to increase the convergence rate of e_1. Now, the error dynamics of the robot manipulator with uncertainties and disturbance can be expressed as

$$\begin{cases} \dot{e}_1 = e_2 - p_1 e_1(t), \\ \dot{e}_2 = \dot{e}_s - \ddot{q} = \dot{e}_s + F_d + B(q)\tau_m + F_{\text{nom}}(q,\dot{q}), \end{cases} \tag{10}$$

where $B(q) = -\widehat{M}^{-1}(q)$, $F_{\text{nom}}(q,\dot{q}) = -\text{B(q)}\left(\widehat{C}(q,\dot{q})\dot{q} + \widehat{G}(q) + \widehat{f}_d\dot{q} + \dot{f}_s(\dot{q})\right)$, and $F_d = -B(q)[F(q,\dot{q},\ddot{q}) + \tau_d]$.

Additionally, because of the system state's large initial deviation, the calculated control torque exceeds the normal operating range of the actuator and is above the saturation zone, which may deteriorate the control performance. The actuator saturation exists for two reasons: one is the saturation limit of the actuator, the other is the existence of integral term. Considering the actuator saturation in FNITSMC, we define the saturated torque as

$$\tau_m = \text{sat}(\tau_c), \tag{11}$$

where τ_c is the calculated control torque and τ_m is saturation level. Subsequently, the saturation depth is deduced as

$$\Delta(\tau_c) = \tau_m - \tau_c. \tag{12}$$

Substituting Equation 12 into Equation 10, one obtains

$$\begin{cases} \dot{e}_1 = e_2 - p_1 e_1(t), \\ \dot{e}_2 = \dot{e}_s - \ddot{q} = \dot{e}_s + B(q)\tau_c + B(q)\Delta(\tau_c) + F_{\text{nom}}(q,\dot{q}) + F_d. \end{cases} \tag{13}$$

It can be observed that the lumped uncertainty F_d is very complicated. It mainly has two parts, the remaining system uncertainties and the external disturbance that is difficult to accurately model. However, the controller is hard to design since F_d is unknown which could sacrifice the accuracy and exacerbate the chattering of the system. On this aspect, we adopt ARBFNN to approximate it.

3 | FNITSMC DESIGN USING ARBFNNS

3.1 | ARBFNN approximation

The RBFNN is widely used to approximate the time-varying nonlinear function due to its excellent approximate capability. In Lee and Choi [30], ARBFNN is proposed and its weights, centers, and widths of Gaussian functions could be online turned in real-time control. As illustrated in Tran and Kang [27], the ARBFNN achieves better approximation and more precise tracking. Therefore, we adopt ARBFNN to approximate the unknown continuous function in F_d. As shown in Figure 1, an RBFNN consists of three layers: the input layer, hidden layer, and output layer.

The input layer $X = \left[e_1^T, e_2^T, q^T, \dot{q}^T\right] \in \Omega_x \subset R^{n_1}$ $(n_1 = 4n)$ is the net input vector.

Hidden layer: In this layer, the Gaussian RBF vector $\Phi(X) = [\Phi_1(X), \Phi_2(X), \cdots, \Phi_l(X)]^T$ is the output of the hidden layer being in the form

$$\Phi_x(X) = \exp\left(-\frac{\|X - c_x\|^2}{2b_x^2}\right), \quad x = 1, 2, ..., l, \tag{14}$$

where $c_x = [c_{x1}, c_{x2}, \cdots c_{xn_1}]$ and b_x are the center and width of the Gaussian function for the neural net x.

Output layer: The output vector $F_d(X)$ of the network can be given as

$$F_d(X) = W^{*T}\Phi(X) + \rho^*, \tag{15}$$

$$W^* = \text{argmin}_W \left\{ \sup_{x \in \Omega_x} \left| F_d(X) - \widehat{W}^T \Phi(X) \right| \right\}, \tag{16}$$

where $W^* \in R^{l \times n}$ and $\widehat{W} \in R^{l \times n}$ are the optimal value and the estimated value of the ARBFNN weight matrix, respectively. $\rho^* \in R^n$ is the model error vector of the ARBFNN approximation.

Note that no acceleration data is used to approximate the uncertain term in F_d. Since the known inertial term related to acceleration has been considered in the nominal dynamic model, the unknown part of the uncertain

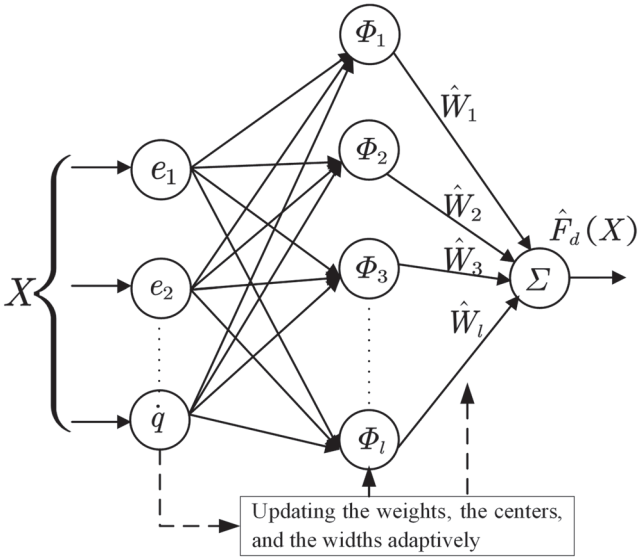

FIGURE 1 The architecture of RBFNN

term composed of acceleration is limited and can be compensated by the robust control terms. Besides, the measurement of acceleration in most robot manipulators is mainly obtained through numerical differentiation, it is commonly inaccurate due to the measurement noise. Additionally, because of the friction and backlash in the robotic actuator, the lumped uncertainty is possibly piecewise continuous function. In Selmic and Lewis [31], sigmoid-jump function is adopted to approximate the discontinuous function. However, the activation function requires the point of discontinuity. It is more suitable for approximating the friction and backlash, rather than the lumped uncertainty. Therefore, in this paper, the abovementioned three-layer ARBFNN is used to approximate the unknown dynamic function.

$$F_d = F_d(X) + \rho^* = W^{*T}\Phi(X) + \rho, \tag{17}$$

where $\rho = \rho^* + \xi_1(X)$ and $\xi_1(X)$ is the bounded piecewise term and ρ^* represents NN approximation error.

Note that the weighting matrix W^*, c_x, and b_x are unknown, which cannot be used for controller design. Then, the adaptive technique is utilized to estimate them.

$$\begin{aligned}\widehat{W} &= \left[\widehat{W}_1, \widehat{W}_2, ..., \widehat{W}_l\right] \\ &= \begin{bmatrix} \widehat{W}_{11} & \widehat{W}_{12} & \cdots & \widehat{W}_{1n} \\ \widehat{W}_{21} & \widehat{W}_{22} & \cdots & \widehat{W}_{2n} \\ \vdots & \vdots & \ddots & \vdots \\ \widehat{W}_{l1} & \widehat{W}_{l2} & \cdots & \widehat{W}_{ln} \end{bmatrix},\end{aligned} \tag{18}$$

$$\begin{aligned}\widehat{c}_x &= [\widehat{c}_{x1}, \widehat{c}_{x2}, \cdots \widehat{c}_{xn_1}], \\ \widehat{b}_x &= \left[\widehat{b}_1, \widehat{b}_2, \cdots \widehat{b}_l\right],\end{aligned} \tag{19}$$

where $\widehat{c}_x$ and $\widehat{b}_x$ are estimated values of c_x and b_x. Let $\widehat{F}_d(X)$ be the estimate of $F_d(X)$, and the $\widehat{F}_d(X)$ is defined as

$$\widehat{F}_d(X) = \widehat{W}^T\Phi(X). \tag{20}$$

3.2 | Controller design

For the dynamic nonlinear system Equation 7 with the lumped system uncertainty, and actuator saturation, this section proposes a robust control scheme using the FNITSM surface to guarantee the finite-time convergence of the tracking error. Substituting Equation 17 into Equation 13, the error dynamics can be written as

$$\begin{cases} \dot{e}_1 = e_2 - p_1 e_1(t), \\ \dot{e}_2 = \dot{e}_s - \ddot{q} = \dot{e}_s + W^{*T}\Phi(X) + B(q)\tau_c + B(q)\Delta(\tau_c) + F_{\text{nom}}(q, \dot{q}) + \rho. \end{cases} \tag{21}$$

Before presenting the sliding mode surface and the control law, the following assumption is given.

Assumption 1. (Nguyen et al. [26]). The lumped ARBFNN approximation error ρ is Lipschitz disturbances, that is, $\rho \leqslant a$, $\dot{\rho} \leqslant b$ with constants a and b unknown.

Then, the following fast nonsingular integral terminal sliding mode (FNITSM) surface [13] is defined

$$\begin{cases} s = e_2 + \int_0^t (r_1\Theta(e_1, \omega_1, \sigma_1, \varepsilon_1) + r_2\Theta(e_2, \omega_2, \sigma_2, \varepsilon_2))\mathrm{d}t, \\ \Theta(e_j, \omega_j, \sigma_j, \varepsilon_j) = \begin{cases} \text{sig}^{\sigma_j}(e_j), & \text{if } |e_j| \leq \varepsilon_j, \\ \text{diag}\left(\varepsilon_j^{\sigma_j - \omega_j}\right)\text{sig}^{\omega_j}(e_j), & \text{if } |e_j| > \varepsilon_j, \end{cases} \end{cases} \tag{22}$$

where

$$\text{j} = 1, 2, \varepsilon_1 = [\varepsilon_{11}, \varepsilon_{12}, \cdots, \varepsilon_{1n}]^T, \varepsilon_2 = [\varepsilon_{21}, \varepsilon_{22}, \cdots, \varepsilon_{2n}]^T, \tag{23}$$

with $\varepsilon_{1i}, \varepsilon_{2i} > 0$ for $i = 1, 2, \cdots, \text{n}$. Besides, $r_1, r_2 \geqslant 0$, $0 < \sigma_2 < 1$, $\sigma_1 = \frac{\sigma_2}{2 - \sigma_2}$, and $\omega_1, \omega_2 \geqslant 1$.

Remark 1. Due to the integral terms, the FNITSM surface promotes zero steady-state error and alleviates chattering of the following proposed control law. Besides, it guarantees the system state converges to zero quickly. It is shown that $\Theta(e_j, \omega_j, \sigma_j, \varepsilon_j)$ is like a barrier function. When the system state is far from the equilibrium state, that is, $|e_j| > \varepsilon_j$, the absolute value of $\Theta(e_j, \omega_j, \sigma_j, \varepsilon_j)$ serves as a barrier variable gain which guarantees the fast convergence. When the system state is close to the equilibrium state, that is, $|e_j| \leqslant \varepsilon_j$, the fractional power term $\Theta(e_j, \omega_j, \sigma_j, \varepsilon_j)$ promotes the system states converge to zero in a finite-time. Note that compared with the work of Li et al.[13], the added p_1 could provide a faster convergence rate for e_1.

To ensure the sliding motion occurs, the derivatives of the sliding mode $\dot{s} = 0$ should be satisfied and written as

$$\begin{aligned}\dot{s} = \dot{e}_s + W^{*\mathrm{T}}\Phi(X) + B(q)\tau_c + B(q)\Delta(\tau_c) \\ + F_{nom}(q,\dot{q}) + \rho + r_1\Phi(e_1,\omega_1,\sigma_1,\varepsilon_1) \\ + r_2\Phi(e_2,\omega_2,\sigma_2,\varepsilon_2)\end{aligned} \tag{24}$$

On the other hand, considering the integral terms in Equation 22 and the input torque limitation of the actuator, the FNITSM surface-based control scheme could cause actuator saturation. Considering this issue, the following auxiliary compensator variable is proposed to compensate for it.

$$\dot{\zeta} = \begin{cases} 0, & \|\zeta\|_2 \leqslant \zeta_0, \\ -k_1\mathrm{sig}^{\alpha_1}(\zeta) - k_2\mathrm{sig}^{\beta_1}(\zeta) + k_3\Delta\tau_c & \\ -\dfrac{\|s^T B(q)\Delta\tau_c\|_1 + 0.5k_3\Delta\tau_c^T\Delta\tau_c}{\|\zeta\|_2^2}\zeta, & \|\zeta\|_2 > \zeta_0, \end{cases} \tag{25}$$

where $\Delta\tau_c$ is defined in Equation 12, $\zeta \in R^{n\times 1}$ is an auxiliary compensator variable vector, $0<\alpha_1<1$, $\beta_1>1$. k_1, k_2, and k_3 are small positive constants and usually tuned by simulations or experiments.

Remark 2. The initial value ζ_0 is chosen according to the saturation limits of the actuator, while k_3 is designed based on the magnitude of actuator saturation depth. Besides, the subitem $k_1 sig^{\alpha_1}(\zeta)$ and $k_2 sig^{\beta_1}(\zeta)$ guarantee the convergence of ζ to avoid possible overcompensation of the actuator saturation. Then, the robot manipulator follows the target trajectory and the required torque gradually decreases below the limited torque of the actuator.

Equating Equation 24 to zero, the following control law can be obtained:

$$\begin{aligned}\tau_{eq} = -B^{-1}(q)\dot{e}_s - B^{-1}(q)(r_1\Theta(e_1,\omega_1,\sigma_1,\varepsilon_1) \\ + r_2\Theta(e_2,\omega_2,\sigma_2,\varepsilon_2) + F_{\mathrm{nom}}(q,\dot{q})),\end{aligned} \tag{26}$$

and

$$\tau_{NN} = -B^{-1}(q)\left(\widehat{W}^T\Phi(X)\right). \tag{27}$$

It can be observed that the perturbation term is not considered in Equation 26. And an auxiliary controller is needed to overcome ARBFNN approximation errors. The common power approach law is designed as

$$\tau_{a1} = -B^{-1}(\mathbf{q})(a_1\cdot s + a_2\mathrm{sig}^{\alpha_2}(s)), \tag{28}$$

where $a_1, a_2 > 0$ and $0<\alpha_2<1$. Besides, to compensate for actuator saturation, the ASO is given as

$$\tau_{a2} = -B^{-1}(\mathbf{q})K_1\zeta - B^{-1}(\mathbf{q})K_2\mathrm{sig}^{\alpha_1}(s), \tag{29}$$

where $0<\alpha_1<1$, $K_1, K_2>0$, $K_1>k_3$.

Thus, the total control law is

$$\tau_c = \tau_{eq} + \tau_{NN} + \tau_{a1} + \tau_{a2}. \tag{30}$$

Theorem 1. *For the robot uncertain dynamics in Equation 7 with the lumped uncertainty and actuator saturation, if the equivalent control law designed in Equation 26–29, the system tracking error e_1 will converge to zero within a bounded convergence time and no occurring of singularity in Equation 30.*

Proof 1. To ensure that the FNITSM surface s and the auxiliary compensator variable ζ can converge in a finite time, the following Lyapunov function is considered:

$$V_1 = \frac{1}{2}s^T s + \frac{1}{2}\zeta^T\zeta, \tag{31}$$

The time derivative of V_1 is

$$\dot{V}_1 = s^T\dot{s} + \zeta^T\dot{\zeta}. \tag{32}$$

Substituting Equation 30 into Equation 32 yields

$$\begin{aligned}\dot{V}_1 &= s^T\dot{s} + \zeta^T\dot{\zeta} \\ &= \mathrm{s}^{\mathrm{T}}\cdot\left[\widetilde{W}^T\Phi(X) - K_1\zeta - K_2 sig^{\alpha_1}(s) + B(q)\Delta\tau_c + \rho - a_1\cdot s - a_2\mathrm{sig}^{\alpha_2}(s)\right] \\ &\quad + \zeta^T\dot{\zeta} \\ &= \mathrm{s}^{\mathrm{T}}\widetilde{W}^T\Phi(X) - s^T K_1\zeta - s^T K_2 sig^{\alpha_1}(s) + s^T B(q)\Delta\tau_c \\ &\quad + \mathrm{s}^{\mathrm{T}}[\rho\text{-}a_1\times \mathrm{s}\text{-}a_2\mathrm{sig}^{\alpha_2}(\mathrm{s})]\text{-}\mathrm{k}_1\zeta^{\mathrm{T}}\mathrm{sig}^{\alpha_1}(\zeta)\text{-}\mathrm{k}_2\zeta^{\mathrm{T}}\mathrm{sig}^{\beta_1}(\zeta) \\ &\quad + \mathrm{k}_3\zeta^{\mathrm{T}}\Delta\tau_c\text{-}\|\mathrm{s}^{\mathrm{T}}\mathrm{B}(\mathrm{q})\Delta\tau_c\|_1\text{-}0.5\mathrm{k}_3\Delta\tau_c^{\mathrm{T}}\Delta\tau_c,\end{aligned} \tag{33}$$

where $\widetilde{W} = W^* - \widehat{W}$ is the error vector of the ARBFNN weight.

Because of the inequalities:

$$\begin{aligned} s^T B(q)\Delta\tau_c &\leqslant \left\|s^T B(q)\Delta\tau_c\right\|_1, \\ \zeta^T \Delta\tau_c &\leqslant \frac{1}{2}\zeta^T\zeta + \frac{1}{2}\Delta\tau_c^T\Delta\tau_c, \\ s^T K_1\zeta &\leqslant \frac{1}{2}s^T K_1 s + \frac{1}{2}\zeta^T K_1\zeta. \end{aligned} \tag{34}$$

According to the above inequalities, we can obtain

$$\begin{aligned} \dot{V}_1 \leqslant & \mathrm{s}^{\mathrm{T}}\widetilde{W}^T\Phi(X) - \frac{1}{2}s^T K_1 s - \frac{1}{2}\zeta^T(K_1 - k_3)\zeta - K_2\left(s^T s\right)^{\frac{\alpha_1+1}{2}} \\ & + s^T[\rho - a_1\cdot s - a_2\mathrm{sig}^{\alpha_2}(s)] - k_1\left(\zeta^T\zeta\right)^{\frac{\alpha_1+1}{2}} \\ \leqslant & -2^{\frac{\alpha_1+1}{2}}K_2\left(\frac{1}{2}s^T s\right)^{\frac{\alpha_1+1}{2}} - 2^{\frac{\alpha_1+1}{2}}k_1\left(\frac{1}{2}\zeta^T\zeta\right)^{\frac{\alpha_1+1}{2}} \\ & + \mathrm{s}^{\mathrm{T}}\widetilde{W}^T\Phi(X) + s^T[\rho - a_1\cdot s - a_2\mathrm{sig}^{\alpha_2}(s)] \\ \leqslant & -\kappa V_1^{\frac{\alpha_1+1}{2}} + Z \end{aligned} \tag{35}$$

where $\kappa = \min\left(2^{\frac{\alpha_1+1}{2}}K_2, 2^{\frac{\alpha_1+1}{2}}k_1\right)$ and $Z = \mathrm{s}^{\mathrm{T}}\widetilde{W}^T\Phi(X) + s^T[\rho - a_1\cdot s - a_2\mathrm{sig}^{\alpha_2}(s)]$. Assume that Z is bounded; then according to Lemma 1, s and ζ will converge in a finite time and the settling time can be calculated as

$$T_s \leqslant \frac{V_1(0)^{1-\frac{\alpha_1+1}{2}}}{\kappa\left(1-\frac{\alpha_1+1}{2}\right)}. \tag{36}$$

The adaptation laws for updating the weights of the ARBANN, the centers, and the widths of the Gaussian functions are designed as

$$\begin{cases} \dot{\widehat{W}} = -\dot{\widetilde{W}} = \Gamma_W\left(\Phi(X)s^T - \|s\|_2\widehat{W}\right), \\ \dot{\widehat{c}} = -\dot{\widetilde{c}} = -\Gamma_c\|s\|_2\widehat{c}, \\ \dot{\widehat{b}} = -\dot{\widetilde{b}} = -\Gamma_b\|s\|_2\widehat{b}, \end{cases} \tag{37}$$

where $\widetilde{c} = c^* - \widehat{c}$ and $\widetilde{b} = b^* - \widehat{b}$ are the error vectors between the optimal value and the estimated value of the center vector and width vector of the ARBFNN, respectively. Γ_W, Γ_c, and Γ_b are positive definite symmetric matrixes.

Define the following Lyapunov function as

$$\begin{aligned} V_2 = & \frac{1}{2}s^T s + \frac{1}{2}\zeta^T\zeta + \frac{1}{2}tr\left(\widetilde{W}\Gamma_W^{-1}\widetilde{W}\right) + \frac{1}{2}tr\left(\widetilde{c}\Gamma_c^{-1}\widetilde{c}\right) \\ & + \frac{1}{2}tr\left(\widetilde{b}\Gamma_b^{-1}\widetilde{b}\right). \end{aligned} \tag{38}$$

The time derivative of V_2 is

$$\begin{aligned} \dot{V}_2 = & s^T\dot{s} + \zeta^T\dot{\zeta} - tr\left(\widetilde{W}^T\Gamma_W^{-1}\dot{\widehat{W}}\right) - tr\left(\widetilde{c}^T\Gamma_c^{-1}\dot{\widehat{c}}\right) - tr\left(\widetilde{b}^T\Gamma_b^{-1}\dot{\widehat{b}}\right) \\ = & \mathrm{s}^{\mathrm{T}}\cdot\left\{\widetilde{W}^T\Phi(X) - K_1\zeta - K_2 sig^{\alpha_1}(s) + B\Delta\tau_c + [\rho - a_1\cdot s - a_2\mathrm{sig}^{\alpha_2}(s)]\right\} \\ & + \zeta^T\dot{\zeta} - tr\left(\widetilde{W}^T\Gamma_W^{-1}\dot{\widehat{W}}\right) - tr\left(\widetilde{c}^T\Gamma_c^{-1}\dot{\widehat{c}}\right) - tr\left(\widetilde{b}^T\Gamma_b^{-1}\dot{\widehat{b}}\right). \end{aligned} \tag{39}$$

Substituting the above adaptation laws Equation 37 to $\dot{V}_2$, one obtains

$$\begin{aligned} \dot{V}_2 = & -s^T K_1\zeta - s^T K_2 sig^{\alpha_1}(s) + s^T B(q)\Delta\tau_c + s^T[\rho - a_1\cdot s - a_2\mathrm{sig}^{\alpha_2}(s)] \\ & - k_1\zeta^T sig^{\alpha_1}(\zeta) - k_2\zeta^T sig^{\beta_1}(\zeta) - \left\|s^T B(q)\Delta\tau_c\right\|_1 - 0.5k_3\Delta\tau_c^T\Delta\tau_c \\ & + k_3\zeta^T\Delta\tau_c + \|s\|_2 tr\left(\widetilde{W}^T\widehat{W}\right) + \|s\|_2 tr\left(\widetilde{c}^T\widehat{c}\right) + \|s\|_2 tr\left(\widetilde{b}^T\widehat{b}\right). \end{aligned} \tag{40}$$

According to the property of the Frobenius norm:

$$\begin{cases} \|s\|_2 tr\left(\widetilde{W}^T\widehat{W}\right) \leqslant \|s\|_2\dfrac{W_{\max}^2}{4}, \\ \|s\|_2 tr\left(\widetilde{c}^T\widehat{c}\right) \leqslant \|s\|_2\dfrac{c_{\max}^2}{4}, \\ \|s\|_2 tr\left(\widetilde{b}^T\widehat{b}\right) \leqslant \|s\|_2\dfrac{b_{\max}^2}{4}, \end{cases} \tag{41}$$

where $W_{\max}$, $c_{\max}$, and $b_{\max}$ are the maximum values of the Frobenius norm of the W^*, c^*, and b^* respectively. Then, we obtain the positive variance constants k_w, k_c, and k_b which satisfy $W_{\max}^2 \leqslant k_w\|s\|_2$, $c_{\max}^2 \leqslant k_c\|s\|_2$, and $b_{\max}^2 \leqslant k_b\|s\|_2$.

According to the above inequalities, one obtains

$$\begin{aligned} \dot{V}_2 \leqslant & -\frac{1}{2}s^T K_1 s - \frac{1}{2}\zeta^T K_1\zeta - K_2\left(s^T s\right)^{\frac{\alpha_1+1}{2}} + s^T[\rho - a_1\cdot s - a_2\mathrm{sig}^{\alpha_2}(s)] \\ & - k_1\left(\zeta^T\zeta\right)^{\frac{\alpha_1+1}{2}} + \|s\|_2\frac{W_{\max}^2}{4} + \|s\|_2\frac{b_{\max}^2}{4} + \|s\|_2\frac{c_{\max}^2}{4} + \frac{1}{2}\zeta^T k_3\zeta \\ \leqslant & -\frac{1}{2}\zeta^T(K_1 - k_3)\zeta - 2^{\frac{\alpha_1+1}{2}}K_2\left(\frac{1}{2}s^T s\right)^{\frac{\alpha_1+1}{2}} - 2^{\frac{\alpha_1+1}{2}}k_1\left(\frac{1}{2}\zeta^T\zeta\right)^{\frac{\alpha_1+1}{2}} \\ & - \left(a_2\|s\|_2^{2\alpha_2+1} - \frac{k_w}{4} - \frac{k_b}{4} - \frac{k_c}{4} - \rho\right)\|s\|_2 - a_1\cdot\|s\|_2^2. \end{aligned} \tag{42}$$

Combining Assumption 1, if $a_2 > \|s\|_2^{(-2\alpha_2-1)}\left(\frac{k_w}{4} + \frac{k_b}{4} + \frac{k_c}{4} + \rho\right)$ and $K_1 > k_3$, one obtains $\dot{V}_2 \leqslant 0$ and $0 \leqslant V_2 \leqslant V_2(0)$. It denotes that $\widetilde{W}$, $\widetilde{c}$, and $\widetilde{b}$ are bounded. Combine Equations 35 and 36, we could conclude that the FNITSM surface s and compensator variable ζ will converge in a finite time. When the sliding mode $s = 0$ is reached after the reaching time T_s and consequently $\dot{s} = 0$ which allows the following equation to determine the error dynamics of the system:

$$\dot{e}_2 + r_1\Phi(e_1,\omega_1,\sigma_1,\varepsilon_1) + r_2\Phi(e_2,\omega_2,\sigma_2,\varepsilon_2) = 0. \quad (43)$$

Then according to Lemma 1, the variable in Equation 43 is local finite-time-stable to the equilibrium point $(e_1,e_2) = (0,0)$ for any given initial condition. Therefore, the ARBFNNs approximation error does not need to converge to zero, and the system error will still be stable. This completes the Proof 1.

The control block diagram of the proposed controller is shown in Figure 2. The overall control block diagram of the robotic manipulator consists of three parts, the functions of which are as follows.

Part A is a FNITSM controller that achieves robust high-precision control of robotic systems under the lumped model uncertainty. It ensures fast finite-time convergence with less chattering.

Part B is a ARBFNN controller, which is used to approximate and compensate for the lumped uncertainty. Benefits from the adaptive laws, the weights, centers, and widths of the ARBFNN can be adjusted in real-time through tracking error. In this way, an ARBFNN-based controller neither requires a time-consuming training process nor laborious parameters turning process. It is suitable for real-time control.

Part C is an ASO controller, which is used to compensate for the actuator saturation. It helps solve the overshoot or instability issues in FNITSMC and promote its performance development.

4 | DESIGN CONTINUOUS APPROACH LAWS

Due to the hysteresis of the discontinuous switching function in time and space, the state trajectory reaches the sliding mode surface and converges to the origin with inevitable chattering. Considering this defect, the boundary layer approach and the sigmoid function are widely adopted to alleviate chattering. When the state trajectory approaches the sliding mode surface, the convergence rate is artificially reduced to provide significant chattering mitigation. However, a direct and simple replacement will cause a tradeoff between the steady error and the effects of removing chattering. Then, literature [32] proposed a continuous fractional-order power (CFOP) approach law. Its state trajectory can eventually converge to the given switching plane and alleviate the inherent chattering problem without sacrificing control accuracy. Besides, in presence of Lipschitz disturbances (not necessarily bounded) and low-frequency disturbance, the super-twisting (STW) algorithm is introduced to serve as a suitable alternative for the slow actuator dynamics [33]. However,

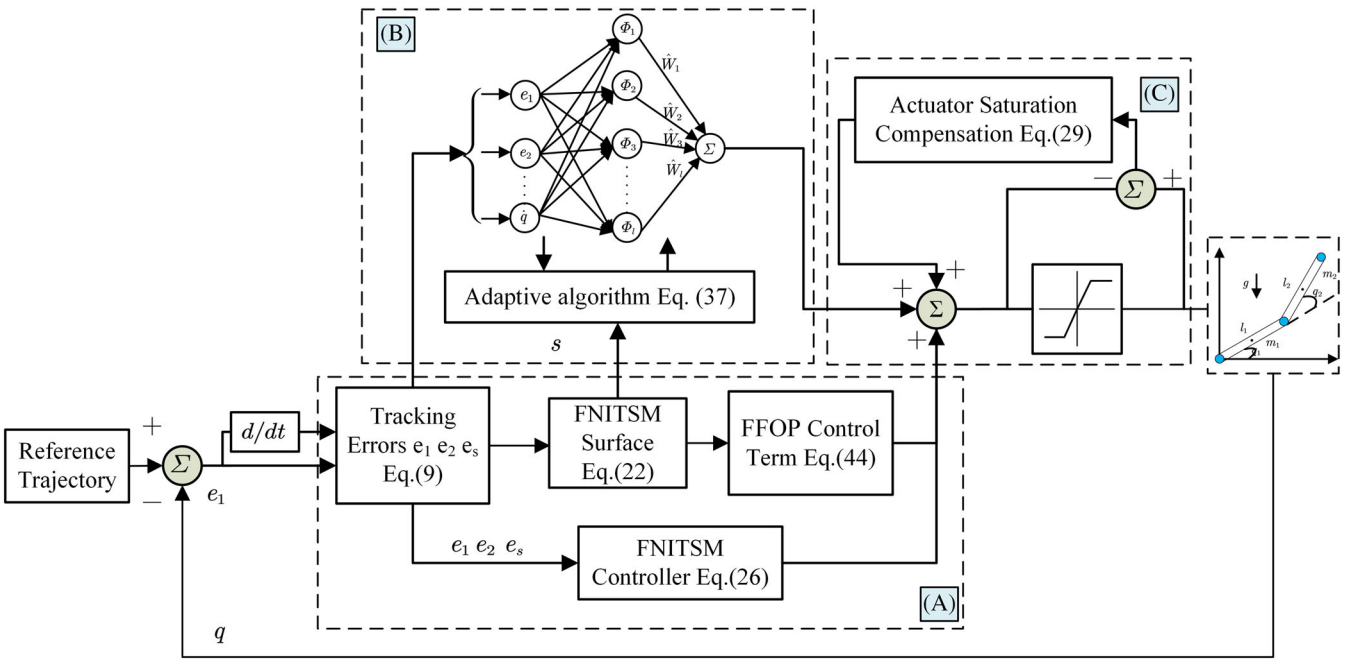

FIGURE 2 Block diagram of the proposed ARBFNN based FNITSMC scheme

these continuous approach laws still require the exact information of the disturbance's upper bound or its time derivative to avoid exacerbating chattering and guarantee the convergence of the sliding mode.

In this section, a novel continuous approach law combining the saturation function and fast fractional-order power (FFOP) approach law is proposed to further improve the control performance of continuous approach law.

Theorem 2. *A novel continuous approach law combining the saturation function and fast fractional-order power (CFFOP) approach law is defined as*

$$\text{①}\ \underline{\mathrm{s}}(\mathrm{t}) = -(\rho_1 \mathrm{s}(\mathrm{t}) + \rho_2 \Xi(\mathrm{s}(\mathrm{t}), \alpha_3, \beta_2, \varepsilon_3)),$$
$$\Xi(s(t), \alpha_3, \beta_2, \varepsilon_3) = \begin{cases} \dfrac{\mathrm{sig}^{\beta_2}(s(t))}{\varepsilon_3^{\beta_2}}, & if\ |s(t)| \leqslant \varepsilon_3, \\ \varepsilon_3^{\beta_2 - \alpha_3} \mathrm{sig}^{\alpha_3}(s(t)), & if\ |s(t)| > \varepsilon_3, \end{cases} \tag{44}$$

with $\varepsilon_3 = [\varepsilon_{31}, \varepsilon_{32}, \cdots, \varepsilon_{3n}]^T$ *and n is the degree of freedom of the robot manipulator. Besides* $0 < \beta_2 < 1$, $\alpha_3 \geqslant 1$, $\varepsilon_{3\mathrm{i}} > 0$, ρ_1 *is gain of the linear term which can suppress the linearly growing disturbance.* $\rho_2 |\Xi(\cdot)| > M_1$, M_1 *is the upper bound of the disturbance. Then the variable* $s(t)$ *in Equation 44 will converge to zero within finite time.*

Proof 2. The proof of the convergence of the NFITSM variable s is similar to Theorem 1; hence, the proof is omitted here for brevity.

Remark 3. The main advantage of the proposed algorithm $\Xi(\cdot)$ is that no demand of the disturbance's upper bound or its time derivative. When the system state $s(t)$ is far from the equilibrium state, that is, $|s(t)| > \varepsilon_3$, the absolute value of $\Xi(s, \alpha_3, \beta_2, \varepsilon_3)$ serves as a barrier variable gain to guarantee a fast convergence rate. When the system state $s(t)$ is close to the equilibrium state, that is, $|s(t)| \leqslant \varepsilon_3$, the fractional power term $\Xi(s, \alpha_3, \beta_2, \varepsilon_3)$ guarantees the state convergence in a finite-time without chattering. Furthermore, the small parameter β_2 can also suppress the chattering to a certain extent [32].

Comparing with the proposed approach law Equation 44, the common FFOP approach laws and CFOP approach law can be expressed as

$$\text{②}\ \underline{\mathrm{s}} = -\rho_1 \mathrm{s} - \rho_2 \mathrm{sig}(\mathrm{s})^{\beta_2},$$
$$\text{③}\ \underline{\mathrm{s}} = -\rho_1 \mathrm{sig}(\mathrm{s})^{\alpha_2} - \rho_2 \mathrm{sig}(\mathrm{s})^{\beta_2},$$
$$\text{④}\ \underline{\mathrm{s}} = -\rho_1 \mathrm{s} - \rho_2 \mathrm{sat}\left(\frac{\mathrm{sig}(\mathrm{s})^{\beta_2}}{\varepsilon^{\beta_2}}\right), \mathrm{sat}\left(\frac{\mathrm{sig}(\mathrm{s})^{\beta_2}}{\varepsilon^{\beta_2}}\right) = \begin{cases} \dfrac{\mathrm{sig}(\mathrm{s})^{\beta_2}}{\left\|\mathrm{sig}(\mathrm{s})^{\beta_2}\right\|}, & |\mathrm{s}| > \varepsilon, \\ \dfrac{\mathrm{sig}(\mathrm{s})^{\beta_2}}{\varepsilon^{\beta_2}}, & |\mathrm{s}| \leqslant \varepsilon. \end{cases} \tag{45}$$

Figure 3 illustrates that case ① (i.e., CFFOP 44) is superior to the other approach laws in terms of the convergence rate. Then, we add high-frequency disturbance $\Delta(t) = 5\sin(t) + 0.5\sin(200\pi t)$, which includes the lumped disturbance and high-frequency measurement noise, to the prototypical dynamic systems ①∼④. Besides, the control outputs of the approach laws are limited to ±30 Nm. The comparison results are depicted in Figure 4. Note that the CFFOP approach law shows less steady-state error and faster convergence rate under same saturation output. On this aspect, the proposed approach law is a simple and effective method and we further demonstrate its performance in following simulation studies.

5 | SIMULATION STUDIES

To demonstrate the proposed control schemes' performance, two simulation studies are conducted in this section. First, to evaluate the robustness of the continuous control scheme, three types of sliding mode controllers are employed to a two-link robot manipulator with model uncertainties, external disturbance, and actuator saturation for comparison. Second, ARBFNN based continuous fast nonsingular integral terminal sliding mode control of a two-link robot manipulator with actuator saturation is presented to evaluate finite-time convergence of the proposed controller and effectiveness of ASO compensation. The turning parameters required for the control laws Equations 48–50 are listed in Table 1. MATLAB/Simulink is used to perform all simulations, and the sampling time is set to 10^{-3} s.

As shown in Figure 5, we consider a two-link robot manipulator for robust finite-time control of the trajectory tracking. The dynamic of the robot manipulator by the Lagrange equation can be given in Equation 6.

The dynamic parameters of the robot manipulator [34] are utilized for simulation. Then, the robotic arm dynamics are given

$$M(q) = \begin{bmatrix} (m_1 + m_2) l_1^2 + m_2 l_2^2 + 2 m_2 l_1 l_2 c_2 + J_1 & m_2 l_2^2 + m_2 l_1 l_2 c_2 \\ m_2 l_2^2 + m_2 l_1 l_2 c_2 & m_2 l_2^2 + J_2 \end{bmatrix},$$

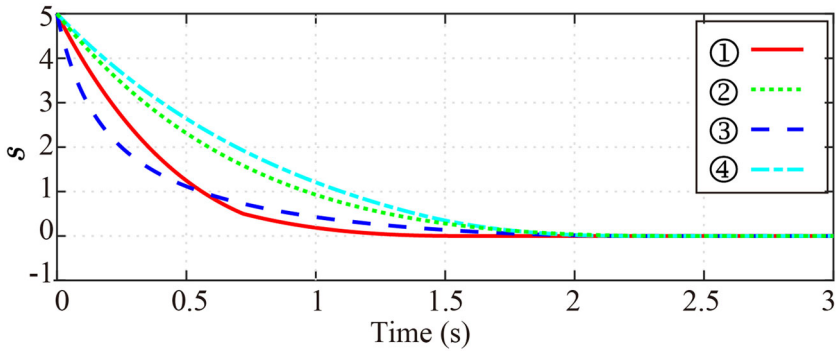

FIGURE 3 The comparison between (44) and fractional power term (45) when $\rho_1 = 1$, $\rho_2 = 1$, $\varepsilon = \varepsilon_3 = 0.5$, $\alpha_3 = 2$, and $\beta_2 = 0.5$

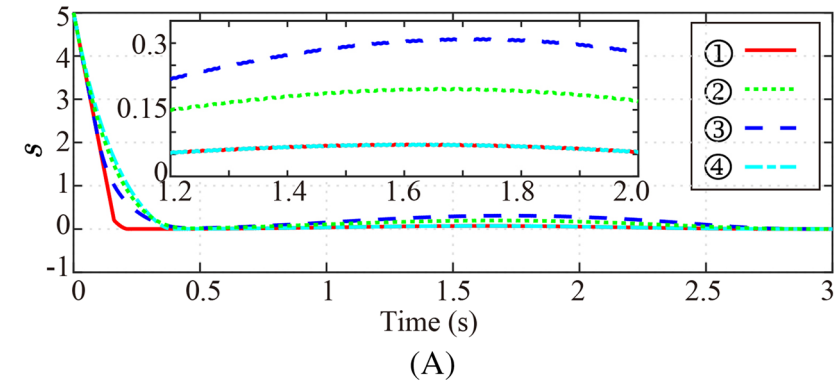

(A)

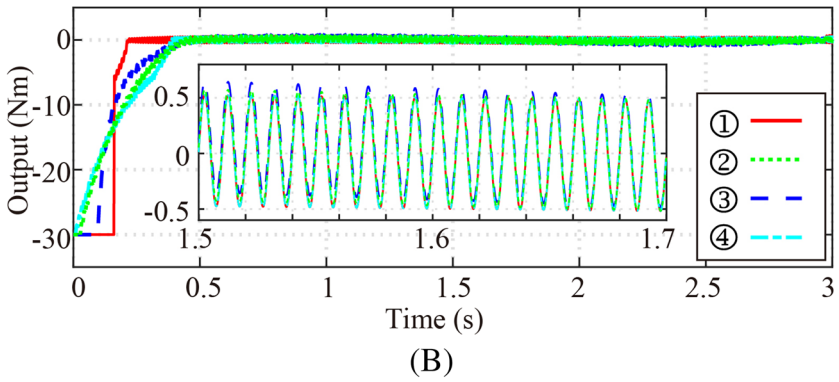

(B)

FIGURE 4 The comparison between (44) and fractional power term (45) when $\rho_1 = 5$, $\rho_2 = 6$, $\varepsilon_3 = 0.2$, $\alpha_3 = 2$, and $\beta_2 = 0.25$. (a) Sliding variable s versus time. (b) Control output of the approach laws

Parameter	Value	Parameter	Value
Error gain p_1	2I	Compensator power β_1	1.5
FNITSM gain r_1	3I	Auxiliary constant ζ_0	0.005
FNITSM gain r_2	1.3I	Auxiliary gain K_1	diag(0.1,1.1)
FNITSM power w_1, w_2	1.2, 1.5	Auxiliary gain K_2	0.1I
FNITSM power σ_1, σ_2	1/3, 1/2	RBFNN gain Γ_W	diag(100,50)
Positive scalar ε_1	[0.2;0.2]	RBFNN gain Γ_c	10I
Positive scalar ε_2	[0.1;0.1]	RBFNN gain Γ_b	20I
Positive scalar ε_4	[0.1;0.1]	CFFOP gain a_3	15I
Compensator gain k_1	0.05I	CFFOP gain a_4	I
Compensator gain k_2	I	CFFOP power β_3	1/3
Compensator gain k_3	0.05I	CFFOP power α_4	2.5
Compensator power α_1	0.8		

TABLE 1 Controllers parameters for the proposed control system

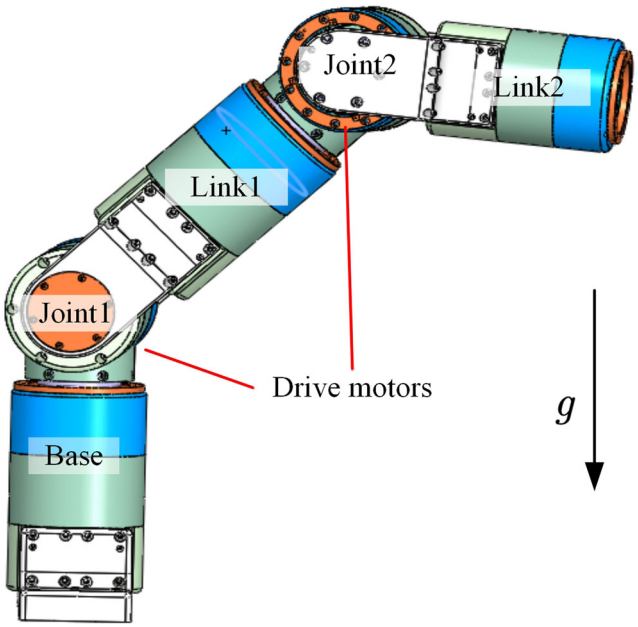

FIGURE 5 The architecture of the two-link robot manipulators

$$C(q,\dot{q})\dot{q}=\begin{bmatrix}-m_2l_1l_2s_2\dot{q}_2^2-2m_2l_1l_2s_2\dot{q}_1\dot{q}_2\\ m_2l_1l_2s_2\dot{q}_2^2\end{bmatrix},$$

$$G(q)=\begin{bmatrix}(m_1+m_2)l_1gc_1+m_2l_2g\cos(q_1+q_2)\\ m_2l_2g\cos(q_1+q_2)\end{bmatrix},$$

where $c_i=\cos(q_i), s_i=\sin(q_i)\,(i=1,2)$. The parameter values are $m_1=0.5\text{kg}$, $m_2=1.5kg$, $l_1=1m$, $l_2=0.8m$, $J_1=5kg\cdot m^2$, and $J_2=5kg\cdot m^2$. $g=9.8m/s^2$ is the acceleration of gravity. Additionally, the unknown dynamics of the manipulator are considered as 20% of the actual dynamics.

$$m_i=\widehat{m}_i+0.2\widehat{m}_i,\quad I_i=\widehat{I}_i+0.2\widehat{I}_i,\quad i=1,2.$$

The desired reference signals are given by

$$\begin{cases}q_{d1}=1.25-\dfrac{7}{5}\exp(-t)+\dfrac{7}{20}\exp(-4t),\\ q_{d2}=1.25+\exp(-t)-\dfrac{1}{4}\exp(-4t),\end{cases}\tag{46}$$

and the external disturbances considered are

$$\begin{cases}\tau_{d1}=2\sin(t)+0.5\sin(200\pi t),\\ \tau_{d2}=2\cos(2t)+0.5\sin(200\pi t).\end{cases}\tag{47}$$

5.1 | Case 1

To better demonstrate the superiority of the proposed control scheme with CFFOP approach law, two other types of terminal sliding mode controllers are also introduced in simulations for comparison, which are adaptive fast nonsingular integral terminal sliding mode control (AFNITSMC) of Li et al. [13] and adaptive nonsingular fast terminal sliding mode control (ANFTSMC) of Boukattaya et al. [34]. In the following comparison simulations, the applied external disturbance is same, and the control inputs are both limited to ±30 N.

The total control law of the proposed CFFOP-FNITSMC scheme becomes

$$\begin{cases}\tau_{c1}=\tau_{eq}+\tau_{ac1},\\ \tau_{ac1}=-a_3s-a_4\Xi(s,\alpha_4,\beta_3,\varepsilon_4),\end{cases}\tag{48}$$

Simulation results are presented in Figures 6–8. The positions of joint1 and joint2 in comparison with the desired trajectory are shown in Figure 6, and the tracking errors and control input signals are illustrated in Figures 7 and 8. We can see that the proposed controller exhibits faster global convergence rate and less chattering than the other controllers. Compared with the AFNITSMC, the CFFOP-FNITSMC scheme shows a faster convergence rate and less overshoot. Besides, the control torques have less chattering in comparison with ANFTSMC. On the other hand, fast transient response requires more energy consumption of the controller and would cause an overshoot (even inevitably oscillation in AFNITSMC). In Case 1, saturation function in Equation 11 is added to tackle the issue.

Besides, three commonly used indicators to illustrate controllers' performance are introduced [15] to compare the tracking performance. The integral of the absolute value of the error (IAE) given by $IAE:=\int_0^{t_f}|e_1(t)|dt$, the integral of the time multiplied by the absolute value of the error (ITAE) given by $ITAE:=\int_0^{t_f}t\cdot|e_1(t)|\,dt$, and the integral of the square value (ISV) of the control input given by $ISV:=\int_0^{t_f}\tau^2(t)dt$, where t_f indicates the total simulation time. The value of IAE and ITAE reflects the convergence of the tracking errors while ISV illustrates the energy consumption of the controller. The comparison results in Figure 9 illustrate that the proposed controller can provide relatively satisfactory control accuracy in terms of convergence rate and energy consumption.

5.2 | Case 2

In order to further demonstrate the effects of the actuator saturation and effectiveness of ASO compensation, we

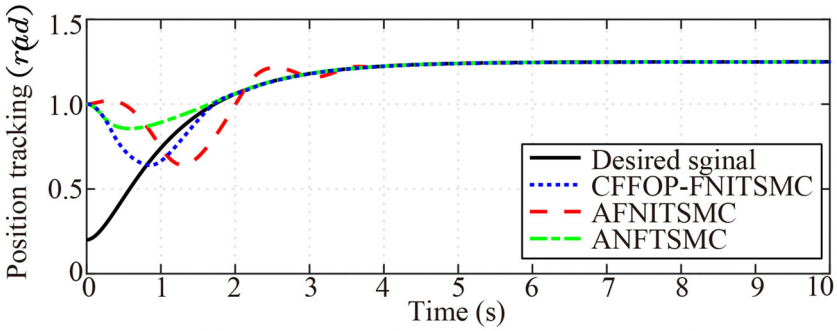

(A) Position tracking performance of joint 1

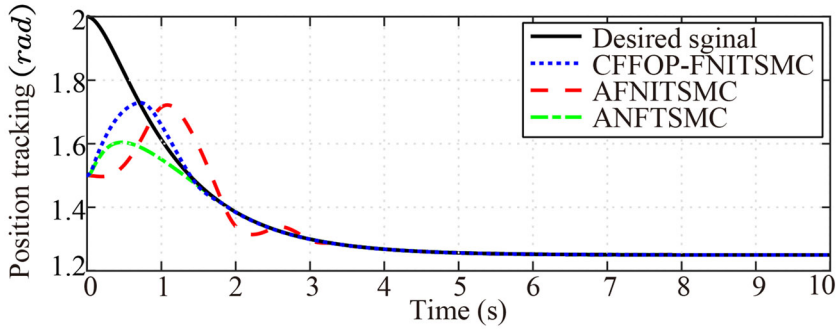

(B) Position tracking performance of joint 2

FIGURE 6 Position tracking performance of joint 1 and 2

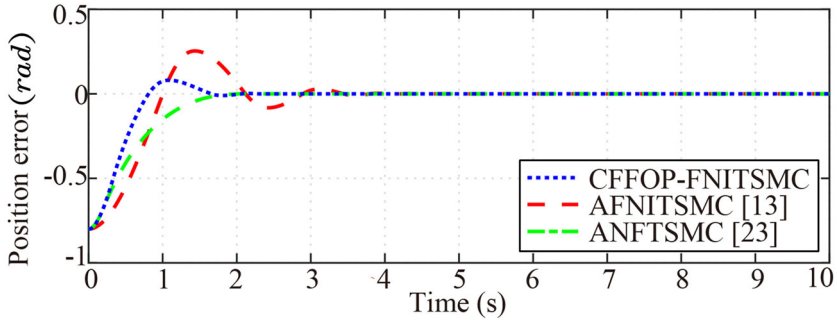

(A) Position tracking error of joint 1

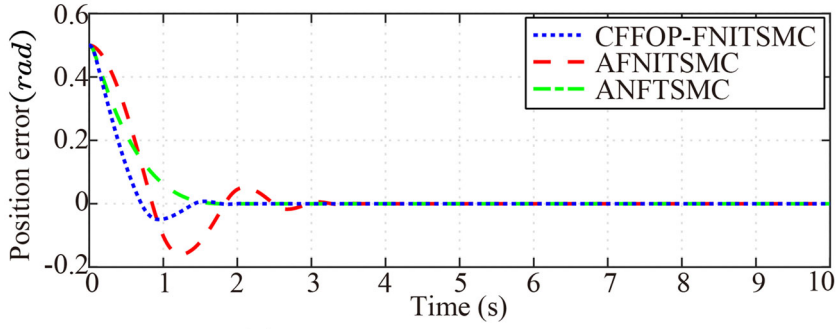

(B) Position tracking error of joint 2

FIGURE 7 Position tracking errors of joint 1 and 2

conduct two other types of CFFOP-FNITSMC schemes with and without ASO for compensation. Additionally, in the presence of relatively large external disturbances, the above controller requires the upper bound of the disturbance to guarantee the sliding is maintained. It would cause chattering in control input since the chattering is not eliminated completely and the upper bound is hard to obtain exactly. Considering this issue,

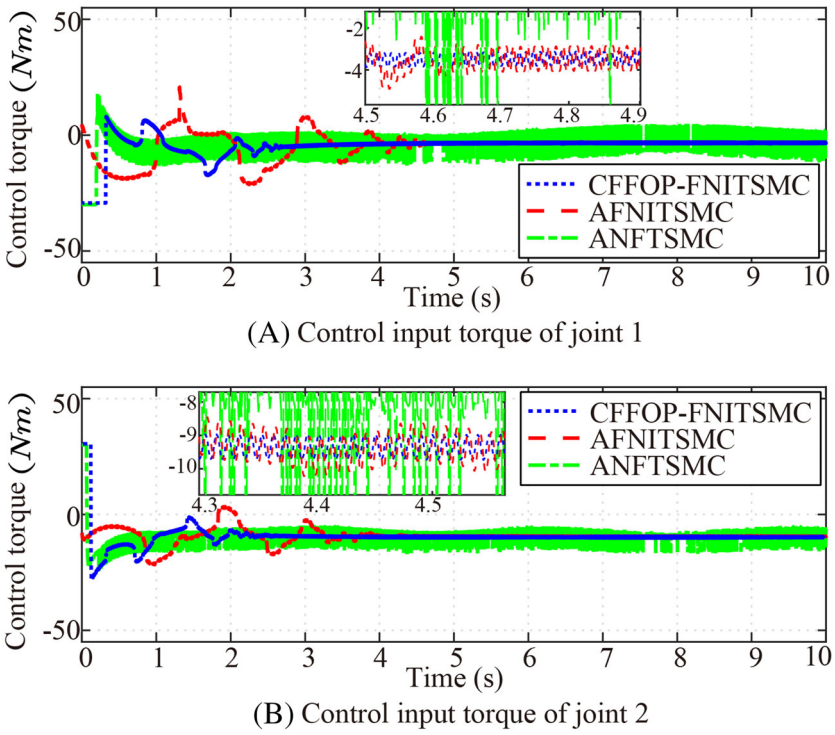

FIGURE 8 Control input torques of joint1 and 2

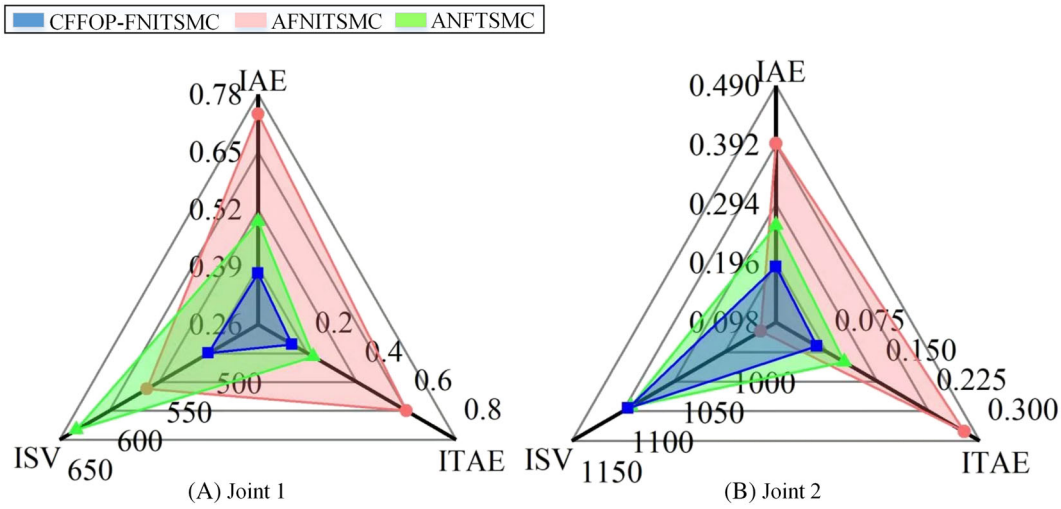

FIGURE 9 Tracking performance of controllers

we use the ARBFNN technique to compensate for the system lumped uncertainty. And the approximation errors are counteracted by robust subitems in controller.

In the following simulation, we assume that the mass and inertia of joint 2 increase to 2.0 kg and 6.5 kg m^2, which represents the load variation of the robot manipulator. Meanwhile, actuator saturation is considered in the control scheme and the control inputs are both limited to ± 30 Nm. And the value of parameter p_1 is reset to diag([8;6]) to increase the convergence rate and the actuator saturation depth. Subsequently, we conduct simulations to compare the performance of different control schemes: the proposed CFFOP-FNITSMC scheme with 21-nodes ARBFNN compensation and ASO compensation (with ASO):

$$\begin{cases} \tau_{c2} = \tau_{eq} + \tau_{ANN} + \tau_{ac1} + \tau_{a2}, \\ \tau_{ac1} = -a_3 s - a_4 \Xi(s, \alpha_4, \beta_3, \varepsilon_4), \end{cases} \tag{49}$$

and the CFFOP-FNITSMC scheme but only with the 21-nodes ARBFNN compensation (without ASO):

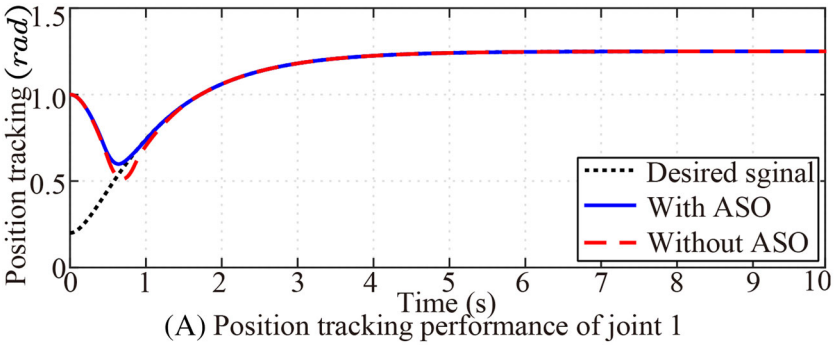

(A) Position tracking performance of joint 1

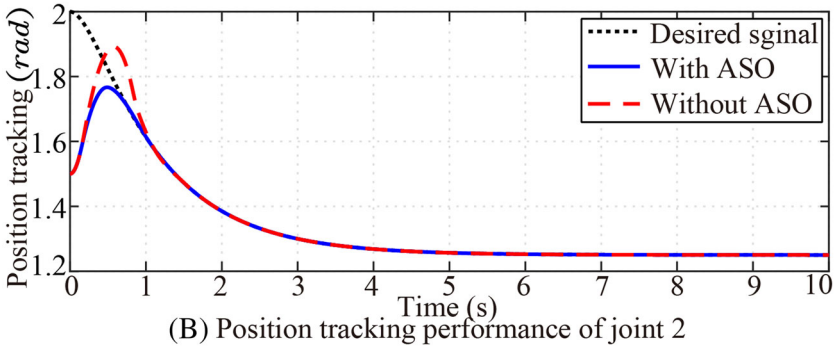

(B) Position tracking performance of joint 2

FIGURE 10 Position tracking performance of joint 1 and 2

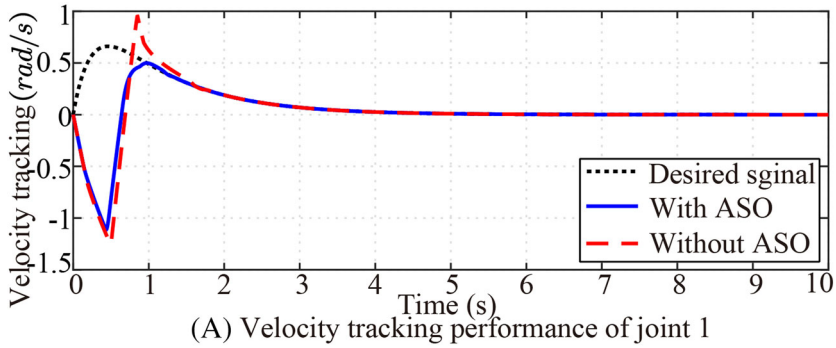

(A) Velocity tracking performance of joint 1

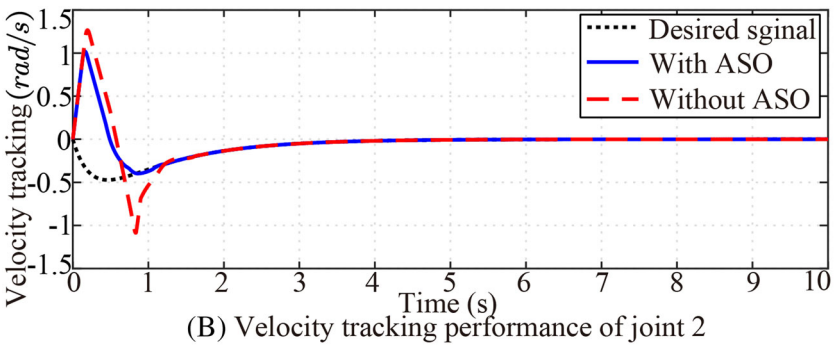

(B) Velocity tracking performance of joint 2

FIGURE 11 Velocity tracking performance of joint 1 and 2

$$\begin{cases} \tau_{c1} = \tau_{eq} + \tau_{ANN} + \tau_{ac1}, \\ \tau_{ac1} = -a_3 s - a_4 \Xi(s, \alpha_4, \beta_3, \varepsilon_4). \end{cases} \tag{50}$$

Simulation results are presented in Figures 10–16. The position and velocity of joint 1 and joint 2 in comparison with the desired trajectory are shown in Figures 10 and 11. And the position and velocity tracking errors are illustrated in Figures 12 and 13. From Figures 10–13, the proposed control law Equation 49 with actuator saturation compensation shows fast transient response and less overshoot. Note that the actuator saturation in the FNITSMC will sacrifice the responding speed of the system and the ASO can compensate for actuator saturation and improve tracking errors'

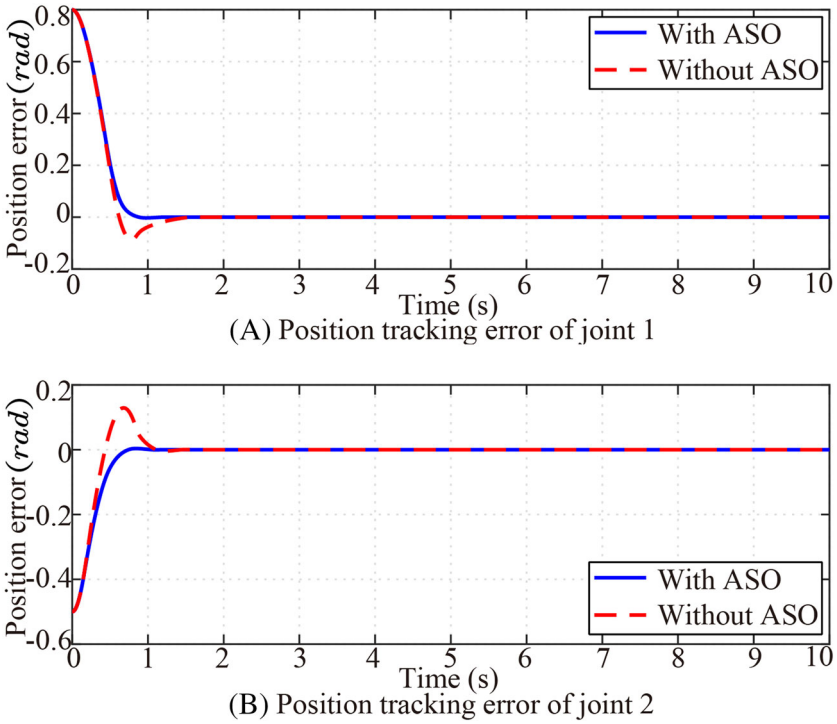

FIGURE 12 Position tracking errors of joint 1 and 2

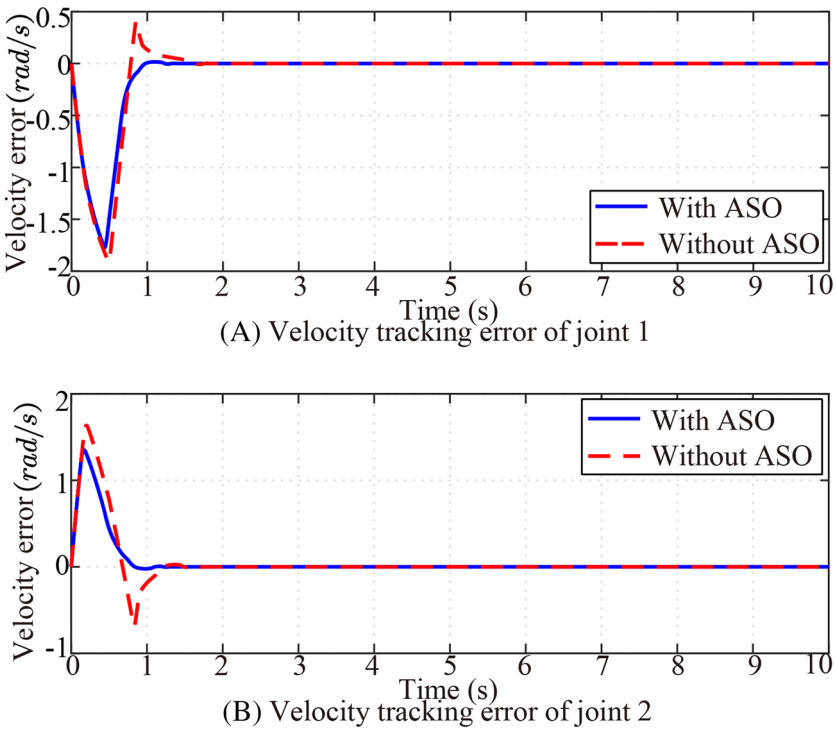

FIGURE 13 Velocity tracking errors of joint 1 and 2

convergence rate. Benefit from the compensation of ARBFNN, the control signals of control law Equation 49 and control law Equation 50 show continuous and chattering free in Figure 14. Figure 15 depicts the convergence of the sliding surface with and without actuator saturation compensation. It can be observed that the ASO greatly improves its transient response. Energy consumption of controllers are presented in Figure 16. From the histogram, we can further conclude that the proposed controller Equation 49 can provide relatively high control accuracy, the faster-responding speed with lower control energy consumption. On this aspect, the

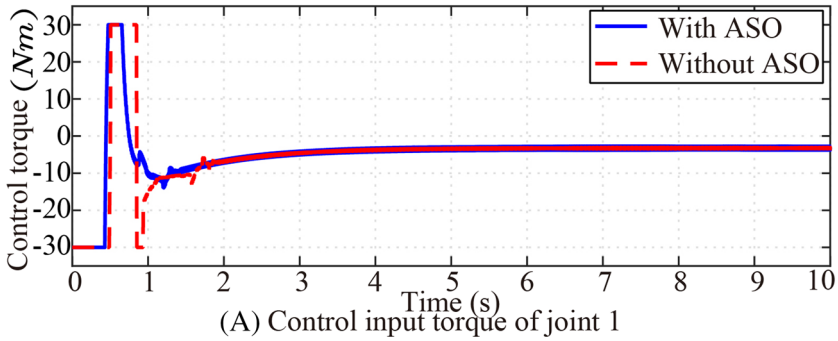

(A) Control input torque of joint 1

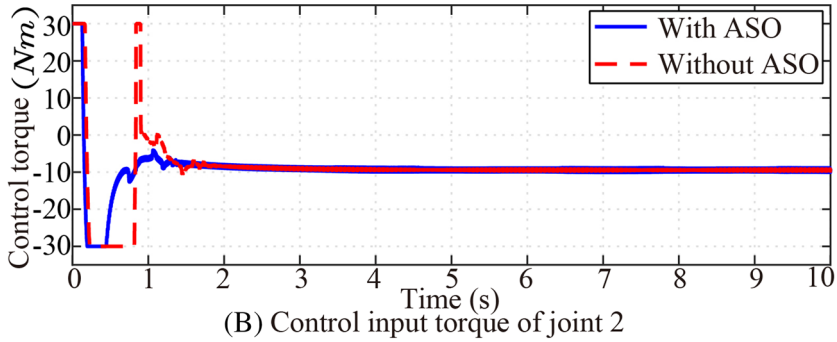

(B) Control input torque of joint 2

FIGURE 14 Control input torques of joint1 and 2

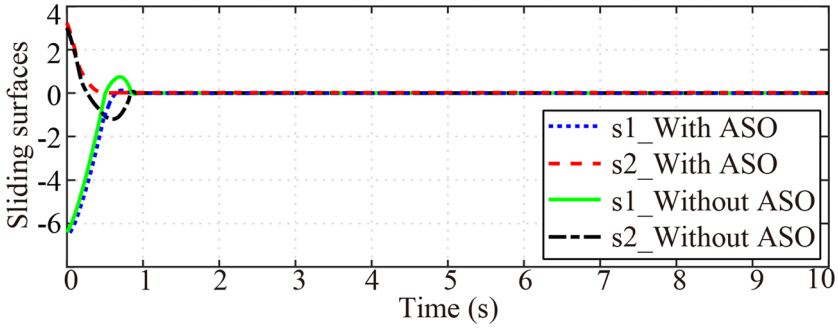

FIGURE 15 Sliding surfaces versus time

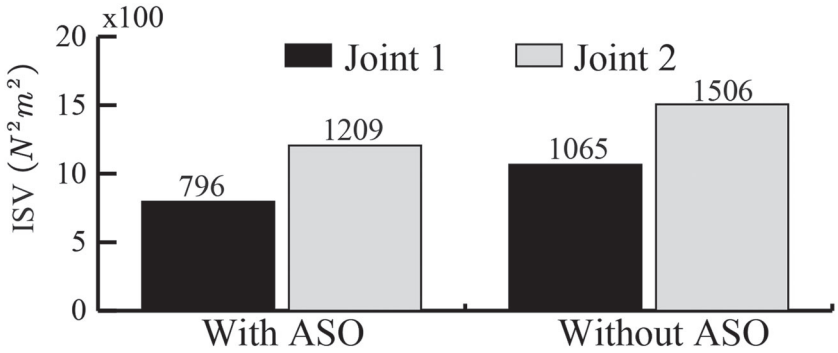

FIGURE 16 Energy consumption of controllers

ASO can help to promote the tracking precision and minimize energy consumption of the integral terminal sliding mode controller. Therefore, the proposed control scheme can be used effectively for robot high-precision tracking control in the presence of the lumped uncertainty and actuator saturation.

6 | CONCLUSION

In this paper, an ARBFNN-based continuous FNITSMC method is proposed for the robust high-precision control of robotic systems. The stability of the proposed controller is proven using Lyapunov theory. Numerical results

show the effect of CFFOP approach law, ARBFNN, and ASO compensation in continuous FNITSMC. And the proposed method could have the following improvements.

- The high-precision tracking control of the robot manipulator can be realized under the lumped system uncertainty with limited and chattering-free control torques.
- Combined with the proposed CFFOP approach law, the controller exhibits continuous and fast finite-time convergence without requiring exact information of the disturbance's upper bound or its time derivative, which makes it easier to be applied to SMC.
- Because the actuator saturation is compensated with ASO and the lumped uncertainty is compensated with the ARBFNN, the proposed control scheme could possess several advantages such as less energy consumption and stronger robustness.

However, further studies would be focused on conducting systematic research on the actuator saturation which probably exists in the finite-time and fixed-time convergence controllers.

ACKNOWLEDGEMENTS

This work is partially supported by the Jilin Scientific and Technological Development Program (20200404204YY) and National Natural Science Foundation of China (11672290).

AUTHOR CONTRIBUTIONS

Yi Li: Software. **huayang Sai:** Investigation. **Mingchao Zhu:** Conceptualization, methodology. **Zhenbang Xu:** Funding acquisition, supervision. **Deqiang Mu:** Formal analysis, project administration.

ORCID

Mingchao Zhu https://orcid.org/0000-0003-3579-7956

REFERENCES

1. S. Jia and J. Shan, *Finite-time trajectory tracking control of space manipulator under actuator saturation*, IEEE Trans. Ind. Electron., **67** (2020), 86–96, https://doi.org/10.1109/TIE.2019.2902789
2. H. Du et al., *Discrete-time fast terminal sliding mode control for permanent magnet linear motor*, IEEE Trans. Ind. Electron., **65** (2018), 16–27, https://doi.org/10.1109/TIE.2018.2815942
3. A. Riani et al., *Adaptive integral terminal sliding mode control for upper-limb rehabilitation exoskeleton*, Control Eng. Pract., **75** (2018), 8–17, https://doi.org/10.1016/j.conengprac.2018.02.013
4. S. Basu Roy, S. Bhasin, and I. N. Kar, *Composite adaptive control of uncertain Euler–Lagrange systems with parameter convergence without PE condition*, Asian J. Control, **22** (2020), 1–10, https://doi.org/10.1002/asjc.1877
5. Y. Feng et al., *Full-order sliding-mode control of rigid robotic manipulators*, Asian J. Control, **21** (2019), 28–36, https://doi.org/10.1002/asjc.1813
6. T. Sun et al., *Semiglobal exponential control of Euler–Lagrange systems using a sliding-mode disturbance observer*, Automatica, **112** (2020), 108677. https://doi.org/10.1016/j.automatica.2019.108677
7. L. Kong et al., *Adaptive fuzzy control for coordinated multiple robots with constraint using impedance learning*, IEEE Trans. Cybern., **49** (2019), 52–63, https://doi.org/10.1109/TCYB.2018.2838573
8. Z. Zhu, Y. Xia, and M. Fu, *Attitude stabilization of rigid spacecraft with finite-time convergence*, Int. J. Robust. Nonlinear Control, **21** (2011), 686–702, https://doi.org/10.1002/rnc.1624
9. S. Ahmed, H. Wang, and Y. Tian, *Robust adaptive fractional-order terminal sliding mode control for lower-limb exoskeleton*, Asian J. Control, **21** (2019), 73–82, https://doi.org/10.1002/asjc.1964
10. Y. Feng, X. Yu, and Z. Man, *Non-singular terminal sliding mode control of rigid manipulators*, Automatica, **38** (2002), 59–67, https://doi.org/10.1016/S0005-1098(02)00147-4
11. L. Yang and J. Yang, *Nonsingular fast terminal sliding mode control for nonlinear dynamical systems*, Int. J. Robust. Nonlinear Control, **16** (2011), 1865–1879, https://doi.org/10.1002/rnc.1666
12. C. S. Chiu, *Derivative and integral terminal sliding mode control for a class of MIMO nonlinear systems*, Automatica, **48** (2012), 16–26, https://doi.org/10.1016/j.automatica.2011.08.055
13. P. Li et al., *Fast nonsingular integral terminal sliding mode control for nonlinear dynamical systems*, Proc. IEEE Conf. Decis. Control, (2014), 39–46, https://doi.org/10.1109/CDC.2014.7040128
14. L. Qiao and W. Zhang, *Trajectory tracking control of auvs via adaptive fast nonsingular integral terminal sliding mode control*, IEEE Trans. Ind. Inform., **16** (2020), 48–58, https://doi.org/10.1109/TII.2019.2949007
15. S. Yi and J. Zhai, *Adaptive second-order fast nonsingular terminal sliding mode control for robotic manipulators*, ISA Trans., **90** (2019), 41–51, https://doi.org/10.1016/j.isatra.2018.12.046
16. D. Li, S. S. Ge, and T. H. Lee, *Simultaneous-arrival-to-origin convergence: Sliding-mode control through the norm-normalized sign function*, IEEE Trans. Automat. Contr., (2021), 1–8, https://doi.org/10.1109/TAC.2021.3069816
17. D. Li et al., *Time-synchronized control for disturbed systems*, IEEE Trans. Cybern., (2021), 1–13, https://doi.org/10.1109/TCYB.2021.3054589
18. S. Zhou et al., *Adaptive neural network control of uncertain MIMO nonlinear systems with input saturation*, Neural. Comput. Appl., **27** (2016), 17–25, https://doi.org/10.1007/s00521-015-1935-7
19. H. T. Chen, S. M. Song, and Z. B. Zhu, *Robust finite-time attitude tracking control of rigid spacecraft under actuator saturation*, Int. J. Control Autom. Syst., **16** (2018), 1–15, https://doi.org/10.1007/s12555-016-0768-1
20. B. Jiang, H. Qinglei, and M. I. Friswell, *Fixed-time attitude control for rigid spacecraft with actuator saturation and faults*,

IEEE Trans. Control Syst. Technol., **5** (2016), 1892–1898, https://doi.org/10.1109/TCST.2016.2519838
21. S. Ahmed, H. Wang, and Y. Tian, *Adaptive fractional high-order terminal sliding mode control for nonlinear robotic manipulator under alternating loads*, Asian J. Control, (2020), 1–11, https://doi.org/10.1002/asjc.2354
22. D. I. Rosas Almeida, J. Alvarez, and J. A. Cantu Cardenas, *Application of the active disturbance rejection control structure to improve the controller performance of uncertain pneumatic actuators*, Asian J. Control, **21** (2019), 99–113, https://doi.org/10.1002/asjc.2026
23. Y. Wu et al., *Performance recovery of dynamic feedback-linearization methods for multivariable nonlinear systems*, IEEE Trans. Automat Contr., **65** (2020), 65–80, https://doi.org/10.1109/TAC.2019.2924176
24. X. Yu et al., *Adaptive fuzzy full-state and output-feedback control for uncertain robots with output constraint*, IEEE Trans. Syst. Man, Cybern. Syst., (2020), 1–14, https://doi.org/10.1109/tsmc.2019.2963072
25. W. He et al., *Reinforcement learning control of a flexible two-link manipulator: An experimental investigation*, IEEE Trans. Syst. Man Cybern. Syst., (2020), 1–11, https://doi.org/10.1109/tsmc.2020.2975232
26. V. T. Nguyen et al., *Adaptive finite-time neural network control for redundant parallel manipulators*, Asian J. Control, **22** (2020), 34–42, https://doi.org/10.1002/asjc.2120
27. M. D. Tran and H. J. Kang, *A novel adaptive finite-time tracking control for robotic manipulators using nonsingular terminal sliding mode and RBF neural networks*, Int. J. Precis. Eng. Manuf., **17** (2016), 63–70, https://doi.org/10.1007/s12541-016-0105-x
28. Y. Wu and R. Lu, *Output synchronization and L_2-gain analysis for network systems*, IEEE Trans. Syst. Man Cybern. Syst., **48** (2018), 5–14, https://doi.org/10.1109/TSMC.2017.2754544
29. Z. Ma and P. Huang, *Adaptive neural-network controller for an uncertain rigid manipulator with input saturation and full-order state constraint*, IEEE Trans. Cybern., (2020), 1–9, https://doi.org/10.1109/tcyb.2020.3022084
30. M. J. Lee and Y. K. Choi, *An adaptive neurocontroller using RBFN for robot manipulators*, IEEE Trans. Ind. Electron., **51** (2004), 1–7, https://doi.org/10.1109/TIE.2004.824878
31. R. R. Selmic and F. L. Lewis, *Neural-network approximation of piecewise continuous functions: Application to friction compensation*, IEEE Trans. Neural Netw., **13** (2002), 45–51, https://doi.org/10.1109/TNN.2002.1000141
32. S. Yu et al., *Continuous finite-time control for robotic manipulators with terminal sliding mode*, Automatica, **41** (2005), 57–64, https://doi.org/10.1016/j.automatica.2005.07.001
33. V. Utkin, *Discussion aspects of high-order sliding mode control*, IEEE Trans. Automat. Contr., **61** (2016), 29–33, https://doi.org/10.1109/TAC.2015.2450571
34. M. Boukattaya, N. Mezghani, and T. Damak, *Adaptive nonsingular fast terminal sliding-mode control for the tracking problem of uncertain dynamical systems*, ISA Trans., **77** (2018), 1–19, https://doi.org/10.1016/j.isatra.2018.04.007

AUTHOR BIOGRAPHIES

Yi Li received his BE degree in the Department of Mechanical and Aerospace Engineering from Jilin University, Changchun, China, in 2017. He is currently pursuing his PhD degree in mechanical engineering and automation with the Changchun Institute of Optics, Fine Mechanics and Physics, Chinese Academy of Sciences, China. His current research interests focus on human-robot interaction, model identification, and the control of robots.

Huayang Sai received his BE degree in School of Mechanical and Electronic Engineering form Northwest Agriculture and Forestry University, Yangling, China, in 2018. He is now a PhD candidate in Mechanical Engineering and Automation, Changchun Institute of Optics, Fine Mechanics and Physics, Chinese Academy of Science, China. He is also currently pursuing the degree with the College of Optoelectronics, University of Chinese Academy of Sciences, Beijing. His current research interests include medical robot, robot impedance control.

Mingchao Zhu received his BS and PhD degrees in the Department of Automation Engineering from the Jilin University, Changchun, China, in 2003 and 2009. Since 2011, he has been an Associate Researcher in Changchun Institute of Optics, Fine Mechanics and Physics, Chinese Academy of Sciences. He is currently engaged in the CAS Key Laboratory of On-orbit Manufacturing and Integration for Space Optics System. His research interests focus on kinematics, dynamics, and control of the robot.

Zhenbang Xu received his BE and PhD degrees in the Department of Theoretical and Applied Mechanics, Chinese Academy of Sciences University, Hefei, China, in 2005 and 2010. He is currently engaged in the CAS Key Laboratory of On-orbit Manufacturing and Integration for Space Optics

System. His research interests include space intelligent robots, multi-dimensional precision adjustment mechanism, and microvibration control.

Deqiang Mu received his BE and ME degrees in the Department of Mechanical and Aerospace Engineering, Jilin University, Changchun, China, in 1982 and 1988, respectively, and PhD degree in Solid Mechanics from Jilin University in 2001. He is currently a professor in the Department of Mechanical Engineering, Changchun University of Technology, Changchun, China. His current research interests include precision machining and testing, machinery manufacturing process, and automation.

How to cite this article: Y. Li, H. Sai, M. Zhu, Z. Xu, and D. Mu, *Neural network-based continuous finite-time tracking control for uncertain robotic systems with actuator saturation*, Asian J Control **24** (2022), 3475–3493. https://doi.org/10.1002/asjc.2744